



Experimental study of a buoyancy-driven instability of a miscible horizontal displacement in a Hele-Shaw cell

F. Haudin, L. A. Riolfo, B. Knaepen, G. M. Homsy, and A. De Wit

Citation: [Physics of Fluids \(1994-present\)](#) **26**, 044102 (2014); doi: 10.1063/1.4870651

View online: <http://dx.doi.org/10.1063/1.4870651>

View Table of Contents: <http://scitation.aip.org/content/aip/journal/pof2/26/4?ver=pdfcov>

Published by the [AIP Publishing](#)

Articles you may be interested in

[Experimental studies of labyrinthine instabilities of miscible ferrofluids in a Hele-Shaw cell](#)
Phys. Fluids **19**, 084101 (2007); 10.1063/1.2756083

[Dispersion relations for the convective instability of an acidity front in Hele-Shaw cells](#)
J. Chem. Phys. **121**, 935 (2004); 10.1063/1.1760515

[Gravitational instability of miscible fluids in a Hele-Shaw cell](#)
Phys. Fluids **14**, 902 (2002); 10.1063/1.1431245

[The threshold of the instability in miscible displacements in a Hele-Shaw cell at high rates](#)
Phys. Fluids **13**, 799 (2001); 10.1063/1.1347959

[Shear instability of two-fluid parallel flow in a Hele-Shaw cell](#)
Phys. Fluids **9**, 3267 (1997); 10.1063/1.869441



Re-register for Table of Content Alerts

Create a profile.



Sign up today!



Experimental study of a buoyancy-driven instability of a miscible horizontal displacement in a Hele-Shaw cell

F. Haudin,¹ L. A. Riolfo,¹ B. Knaepen,² G. M. Homsy,³ and A. De Wit¹

¹*Nonlinear Physical Chemistry Unit, Faculté des Sciences, CP 231, Université Libre de Bruxelles (ULB), 1050 Brussels, Belgium*

²*Statistical and Plasma Physics Group, Faculté des Sciences, CP 231, Université Libre de Bruxelles (ULB), 1050 Brussels, Belgium*

³*Department of Mechanical Engineering, University of British Columbia, Vancouver, British Columbia V6T1Z4, Canada*

(Received 8 June 2013; accepted 12 February 2014; published online 15 April 2014)

When a given fluid displaces another less viscous miscible one in a horizontal Hele-Shaw cell, the displacement is stable from the viscous point of view. Nevertheless, thin stripes perpendicular to the moving interface can be observed in the mixing zone between the fluids both in rectilinear and radial displacements. This instability is due to buoyancy effects within the gap of the cell which develop because of an unstable density stratification associated with the underlying concentration profile. To characterize this buoyancy-driven instability and the related striped pattern, we perform a parametric experimental study of viscously stable miscible displacements in a horizontal Hele-Shaw cell with radial injection. We analyze the influence of the flow rate, the thickness of the gap, and the relative physical fluid properties on the development and characteristics of the instability. © 2014 AIP Publishing LLC. [<http://dx.doi.org/10.1063/1.4870651>]

I. INTRODUCTION

Hydrodynamic instabilities of interfaces impact numerous applications from oil recovery to CO₂ sequestration to name a few. It is classically known that when a fluid 1 of density ρ_1 and viscosity μ_1 is injected with a given velocity into a miscible fluid 2 of density ρ_2 and viscosity μ_2 , various convective instabilities may be observed. From the viscous point of view, if $\mu_1 < \mu_2$, viscous fingering triggered by the unfavorable mobility gradient between the two fluids can deform the interface into fingers, the morphology of which depends on the relative viscosity, density, and rheological characteristics of both fluids.¹ In a gravity field, if the more dense fluid lies on top of the less dense one, the horizontal interface is buoyantly unstable because of a Rayleigh-Taylor instability and related “density fingering” can be observed.^{2–4} In vertical displacements, such viscous and buoyancy effects can either cooperate to stabilize or destabilize the flow⁵ or, on the contrary, compete, in which case there is a critical injection velocity above which there is an instability.¹

In horizontal systems, the density jump is in the direction perpendicular to gravity and the stability of the interface is classically considered to depend only on the viscosity difference: viscous fingering can be observed when the less viscous fluid is injected into the more viscous one while the reverse displacement is viscously stable. The influence of density differences across the miscible interface on the viscous fingering pattern has been recently addressed by both linear stability analysis⁶ and nonlinear simulations⁷ of the full 3D Stokes problem. It has been shown that a buoyancy-driven instability can act within the gap of the cell on the upper side of the finger.

No systematic study has been devoted to analyze buoyancy effects in the reverse viscously stable case, even though instabilities of viscously stable horizontal displacements taking the form of very thin stripes developing perpendicular to the interface have been reported. Obernauer⁸ has observed such stripes in a horizontal Hele-Shaw cell where water is injected from a hole into dyed water and

flows out from another hole. It was conjectured that this instability was due to the slight difference of density between the two liquids. Similar patterns have also been studied in horizontal rectilinear displacements in Hele Shaw cells for dyed aqueous solutions of glycerine injected in water.⁹ It was noted that the stripes exist for a gap width of 0.5 mm but vanish using a gap of 0.25 mm. Moreover, their onset time decreased as the density difference across the interface increased while increasing the viscosity or decreasing the injection speed had a stabilizing effect. These stripes were attributed to a buoyancy-driven instability due to a locally unfavorable density stratification resulting from the velocity profile within the gap (similarly to buoyancy effects seen in gravity currents with external flow¹⁰). For radial injections, similar stripes are observed to grow radially in experiments done with cupric sulfate injected in dyed water in a Hele-Shaw cell.¹¹ Even if there is only a small surface tension between the two solutions, the authors give an interpretation of the pattern in terms of a Marangoni effect. To the best of our knowledge, there is currently no direct experimental proof that the observed thin stripe patterns are due to a buoyancy effect and no systematic experimental study has been made to characterize them in detail. There is however increased interest in understanding the properties of such thin stripes either to suppress them or to avoid confusing them with other patterns due to other instabilities. Recent work has indeed demonstrated that chemical reactions that change the viscosity of polymer solutions^{12–14} can generate patterns at the interface between miscible solutions even in the viscously stable case of a more viscous injected fluid displacing a less viscous one. In such reaction-induced viscous fingering,¹⁴ the pattern-forming role played by reactions modifying the viscosity *in situ* can only be appreciated if the underlying non-reactive displacement is stable, which is not trivial when the above mentioned stripes come into play. Similarly, striped patterns have recently been evidenced experimentally in reactive systems when a pellet of copper sulfate is immersed in a sodium oxalate solution.¹⁵ A precipitate in the form of a striped pattern is observed to grow radially. Such stripes also appear when the copper sulfate solution is pumped radially from below into a sodium oxalate solution covered to avoid evaporation. The authors of this study conjecture that the stripes are manifestations of buoyantly driven convection. Such a hypothesis calls for a detailed characterization of the equivalent non-reactive displacements to analyze when buoyancy-driven stripes can indeed appear and if so, how their properties can control the precipitation pattern.

In this context, we experimentally study viscously stable miscible displacements of one fluid by another miscible, more viscous and denser one inside a Hele-Shaw cell, tuning the relative viscosity and density difference across the interface by modulating the composition of both fluids. We first demonstrate, using a rectilinear displacement, that stripes developing in horizontal displacements vanish if the cell is vertical, which proves that the origin of these stripes is indeed related to the orientation of the density difference with respect to gravity. We discuss the possible instability scenario in terms of a buoyancy-driven instability inside the gap of the cell and discuss the analogy with a Rayleigh-Bénard instability in the presence of a shear in order to explain the direction of the stripes with respect to the direction of the fluid motion. We next analyze experimentally the properties of these stripes in a radial injection as a function of the injection speed, gap width of the cell, and relative density and viscosity differences between the two fluids. We show that the buoyancy-driven stripes develop with an onset time that depends on the relative properties of the liquids, which allows the control of the development of the instability and its influence on fluid mixing.

The article is organized as follows: Section II presents the phenomenon to be studied, shows that it is related to a buoyancy effect, and provides a probable mechanism of the instability. In Sec. III, we present details of the experimental set-up for radial injections. The evolution of the pattern over time as well as the influence of the flow rate q are presented in Sec. IV. In Sec. V, we characterize the dependence of the wavelength of the pattern on the gap width b while keeping the ratio q/b constant. Section VI is dedicated to configurations where differences in viscosity between the two fluids are negligible in order to better illustrate that the destabilizing mechanism under study is due solely to buoyancy effects. The onset time of the instability and the wavelength of the pattern are studied as functions of the relative difference of density between the fluids or for different viscosities $\mu_1 \approx \mu_2$. Finally, in Sec. VII, we present a summary of the findings and conclusions are drawn.

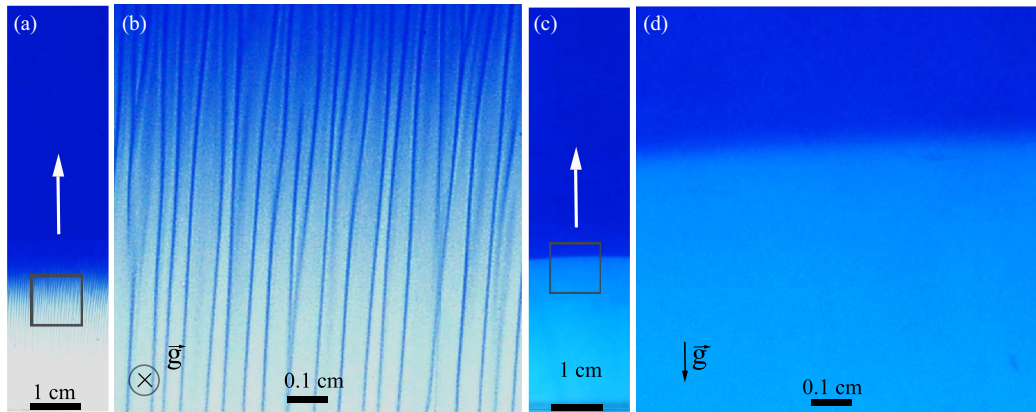


FIG. 1. (a) Striped pattern observed in a horizontal linear displacement of dyed water by a miscible aqueous solution of glycerol 20 wt.%. (c) In a vertical upward injection, the displacement is stable. (b) and (d) show an enlargement of the square in (a) and (c), respectively. The white arrow indicates the direction of injection.

II. BUOYANCY-DRIVEN INSTABILITY

A. Experimental observations

If a viscous solution of 20 wt.% glycerol in water is injected into dyed water from one lateral side of a rectangular cell^{9,16} at a constant speed U , the miscible displacement is stable from a viscous point of view as the viscosity decreases along the direction of motion. Nevertheless, if the cell is horizontal, a pattern with very thin stripes regularly spaced in the direction of the flow develops in the mixing zone between the two fluids (see Figs. 1(a) and 1(b)). No stripes are observed in an upward displacement in a vertical cell (Figs. 1(c) and 1(d)) which proves that the instability in horizontal cells is driven by buoyancy effects. Note that to demonstrate the role of buoyancy in this way, it is necessary to use a cell with a rectilinear injection because it is not possible to proceed the same way with a cell with radial injection. In the latter case, there would indeed be an asymmetry between the upper and the lower part of the cell.

B. Mechanism proposed: Destabilization due to convection

To explain the origin of the stripes visible in Figs. 1(a) and 1(b), let us consider the flow developing in the gap between two plates of a horizontal Hele-Shaw cell upon a displacement of a fluid 2 by a miscible fluid 1 in the viscously stable situation where $\mu_1 > \mu_2$ (Fig. 2(a)). In most cases, the injected more viscous fluid is also the denser one such that $\rho_1 > \rho_2$. A buoyancy-driven instability can then locally develop on the lower part of the concentration profile advected by the parabolic velocity profile, where the denser fluid overlies the less dense one (Figs. 2(b) and 2(c)). Similarly if the displaced fluid is denser than the displacing one, the destabilization due to buoyancy can occur on the upper part of the profile so that the system is always unstable from a buoyancy point of view. As a result, a set of convection rolls develop in the (x, z) plane spanning the thickness of the gap (Fig. 2(c)). From above (along z), these rolls are seen as parallel stripes perpendicular to the miscible interface (i.e., parallel to the y direction in Fig. 2(a)), in agreement with the experimental observations.

To understand the orientation of the stripes with respect to the mean flow motion, direct analogy can be made with buoyancy-driven thermal Rayleigh-Bénard convection. For Rayleigh-Bénard in static layers, it is well known that convection rolls develop in the layer of liquid when the thermal Rayleigh number is larger than a given threshold. A similar criterion based on a solutal Rayleigh number holds if the density stratification is due to concentration gradients. If, in addition to the unstable stratification, there is an imposed parallel shear flow, it is also well known that the effect of the flow is to orient the convection cells into streamwise oriented longitudinal rolls, as discussed in classic papers by Deardorff¹⁷ and by Gage and Reid.¹⁸ The mechanism responsible for this

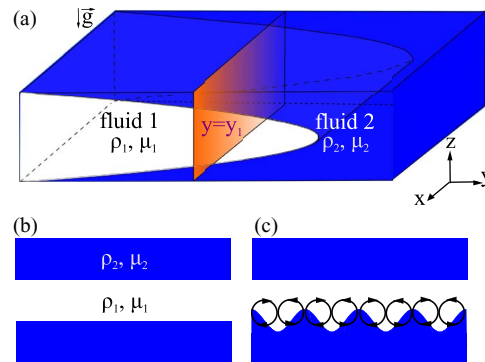


FIG. 2. (a) 3D sketch of the velocity profile in the rectilinear displacement of two miscible fluids in a horizontal Hele-Shaw cell, (b) fluid stratification in the (x, z) plane at an arbitrary position $y = y_1$ shown by the transverse (orange) plane, and (c) qualitative development of convection rolls due to a buoyancy-driven instability of the lower unstable stratification of the denser solution on top of the less dense one.

orientation selection is that the imposed flow and the unstable stratification do not interact if the rolls are oriented in the streamwise direction, while there is a penalty and a higher Rayleigh number required for transverse rolls, as they must overcome the advection in the flow direction in order to persist.

Similar considerations of mode selection hold for the case of flow in Hele-Shaw cells. As shown schematically in Fig. 2(a), an initially vertical density front will be advected and stretched by the underlying Poiseuille flow while simultaneously spreading vertically as a result of diffusion. As sketched in Fig. 2(b), this produces a vertical stratification in which the lower density layer is gravitationally unstable when the upper displacing fluid is denser than the lower displaced one (the upper layer being unstable should the situation be reversed). The situation is slightly more complicated than treated in the classic papers referenced above, as the density stratification depends on both time and spatial location in the direction of flow. However, the same basic mechanisms express themselves, leading to streamwise oriented rolls, as sketched in Fig. 2(c) for the case in which the displacing fluid is the more dense.

These general considerations are substantiated in the very recent paper by Talon *et al.*⁶ While these authors include the effect of unstable viscosity ratios, the findings in their work that are most relevant here are as follows. Using direct numerical simulation of the Stokes equations for a Hele-Shaw flow, they find that the density profiles produced by the parallel flow and depicted schematically in Fig. 2(a) reach a final quasi-steady state in which the variation of the stratification in the flow direction is much weaker than that in the vertical direction. Using these numerically determined base states, they formulate and solve the linear stability problem for a sequence of quasi-steady and quasi-parallel base states. The resulting study shows that, over a very wide range of parameters, longitudinal rolls (their β modes) are always significantly more unstable than transverse modes, the latter being damped or occasionally very weakly unstable for the range of Rayleigh numbers considered. Thus while the details of the flow fields, the range of parameters, and the property ratios considered therein are different than those of our experiments, this work shows that the mechanisms identified by the classical papers cited above^{17,18} are robust, and it substantiates our hypothesis that the striped patterns are buoyancy-driven instabilities that are oriented in the flow direction by the nearly parallel flow in the gap of the Hele-Shaw cell.

In the case of radial injection, the velocity field \vec{v} responsible for the shear is a function of both of the radial distance from the injection point and the vertical direction z . In the creeping flow regime, this velocity profile can be computed analytically.^{19,20} Along the z direction, the profile is parabolic whereas it decays as $1/r$ with the radial coordinate. Explicitly, the expression of radial velocity reads

$$u_r(r, z) = \frac{3q}{8\pi b^3 r} \left(\frac{b^2}{4} - z^2 \right), \quad (1)$$

where q is the flow rate and the walls of the cell are located at $z = \pm \frac{b}{2}$. Neglecting diffusion, the miscible interface between the fluids then adopts a profile in the thin dimension that at any instant of time consists of a section of an ellipse (see the Appendix).

The relative strength of advection and diffusion can be quantified by the Péclet number defined as

$$Pe = \frac{Ub}{D}, \quad (2)$$

where D is the molecular diffusion coefficient of the solute contributing to the density changes and U is a characteristic speed defined for a given radius r as

$$U = \frac{q}{2\pi br}, \quad (3)$$

which gives a Péclet number varying as $1/r$:

$$Pe(r) = \frac{q}{2\pi r D}. \quad (4)$$

This shows that, for a radial displacement, the effects of diffusion become relatively stronger in the course of time because the displacement speed decreases away from the injection point.

If the hypothesis of a buoyancy-driven instability of the density profile stretched in the gap is correct, one expects to characterize the problem in terms of a Rayleigh number Ra which we define as

$$Ra = \frac{\Delta\rho g \mathcal{L}^3}{\mu D}. \quad (5)$$

Here \mathcal{L} is the characteristic length of the mixing zone in the stretched profile over which the density difference $\Delta\rho = \rho_t - \rho_b$ is applied, where ρ_t and ρ_b are the densities of the denser solution at the top and of the less dense one at the bottom ends, respectively, of the density profile while $\mu = (\mu_1 + \mu_2)/2$ is the average of the dynamical viscosity of the two fluids and g is the gravitational acceleration.

Note that, in the present problem, the length \mathcal{L} over which the density contrast develops is a function of time. Indeed, in the course of time, the mean flow stretches the density interface from being vertical at short times to nearly horizontal at longer times, a situation susceptible to buoyancy-driven instabilities. In the case of a Rayleigh-Taylor instability, i.e. for an unfavorable (denser on top) discontinuous jump in density across a sharp horizontal interface, the stratification is always unstable and there is no critical density difference. In the stretched profile considered here (Fig. 2(a)) and in the presence of diffusion and viscous damping, a vertical gradient in density develops in the miscible mixing zone between the two end values ρ_t and ρ_b . The problem is thus analogous to a Rayleigh-Bénard problem with a linear density profile extending over a vertical extent \mathcal{L} growing in time and is then characterized by a threshold value of Ra above which the buoyancy-driven instability sets in.

The Rayleigh number then controls two key aspects of the convection: the onset time and the wavelength of the pattern. Regarding the first of these, the larger the Rayleigh number above the threshold, the larger the growth rate of the instability, and the shorter the onset time. At the same time, the wavelength that is manifest will be approximately that of maximum growth rate, which is known to be only a weak function of the Rayleigh number. Thus, as formula (5) shows, this implies that the system should be more unstable if the density difference $\Delta\rho$ between the two fluids is increased at fixed μ . Similarly, if the density contrast is kept fixed and the viscosity increased, the Rayleigh number is decreased and one expects the system to be more stable. The gap width b does not come into play in the problem as long as $\mathcal{L} \ll b$ which is expected to be true at sufficiently large Péclet numbers and sufficiently short times.

As for the influence of the flow rate q , looking at the formula (1) for the velocity, one sees that the larger the flow rate the faster the density front gets elongated and can then be destabilized. We expect however that the flow rate must be larger than a critical value for destabilization to occur.

Indeed, if q is too small, the relevant Pe is small and diffusive mixing will homogenize the two fluids in the gap faster than injection stretches the profile and no instability is expected.

Let us now confront these various predictions with experimental results.

III. EXPERIMENTAL SET-UP

Our parametric study is performed in a Hele-Shaw cell with radial injection. The Hele-Shaw cell is made of two square plexiglass plates (215 mm \times 215 mm \times 8 mm) separated by a plastic spacer, the thickness of which can be varied and is always less than a millimeter. The fluid is injected from the bottom at the center of the lower plate through an injection valve connected to a syringe pump providing a controlled injection rate (Razel syringe pump). Seen from above the injection valve is a black disk of radius 0.9 cm. For all the experiments, time $t = 0$ corresponds to the last picture before the injected solution appears beyond the black disk of the injection valve. The fluid injected is a mixture in variable concentration of glycerol and distilled water. In some experiments, sucrose solutions are also used or sucrose is added to the glycerol solutions to induce small changes of density. The density is measured with a densimeter at room temperature (between 22.2 and 24.7 °C). Then the viscosity is extrapolated from the measured density using the data²¹ available in the literature at 20 °C. The cell is initially filled with solutions dyed with Trypan blue at a concentration 0.06 wt.% which is assumed not to change the properties of the fluid (diffusion, density, viscosity). It has been checked that the difference of density induced by adding the dye to water is of the order of $\Delta\rho = \rho_1 - \rho_2 = 10^{-4}$ g cm⁻³ at room temperature and is not sufficient to trigger destabilization by a buoyancy effect in our experimental conditions (radial geometry and given range of flow rates), contrary to what was observed by Obernauer⁸ and Maes⁹ for other geometries. The dynamics of the fluid is recorded with a reflex digital camera (Nikon D300) with a macro lens at the frame rate of 1 picture per second. Let us first start with a description of the pattern and of the effect of changing the flow rate.

IV. THIN STRIPES AND INFLUENCE OF THE FLOW RATE

A. Thin stripe pattern

We first consider the case where an aqueous solution of 20 wt.% of glycerol is displacing radially dyed water. The parameters of this reference experiment are reported in Table I. Both density and viscosity differences exist between the two fluids as the injected glycerol solution is denser and more viscous than water. Thus the radial displacement is stable from a viscous point of view, yet a striped pattern evolving with time is quickly observed close to the miscible interface (Fig. 3), similar to what is seen in the rectilinear displacements of Fig. 1.

The first signs of destabilization in the form of radial filaments are visible around $t = 3$ s. In the following, this time necessary for the instability to develop will be referred to as the onset time, t_{onset} . At $t = 4$ s, the pattern is well developed and, later on, it becomes much more visible and extends radially over a larger region. An important feature of the dynamics is the fact that, after a given time or equivalently beyond a given radius, the filaments start splitting, leading to stripes with smaller spacing beyond a certain distance from the injection point. For larger times (i.e., larger radii) not shown in Fig. 3, the relative effect of diffusion to advection becomes larger; in other words the Péclet number Pe decreases, and the stripes become less discernable.

TABLE I. Parameters of the reference experiment of Fig. 3. C_1 is the percentage in mass of glycerol and $\Delta\rho = \rho_1 - \rho_2$.

q (mL/min)	b (mm)	C_1 (wt.%)	ρ_1 (g cm ⁻³)	ρ_2 (g cm ⁻³)	$\Delta\rho/\rho_1$	μ_1 (cP)	μ_1/μ_2
6.48	0.51	20	1.0479	0.9998	46×10^{-3}	1.8	0.56

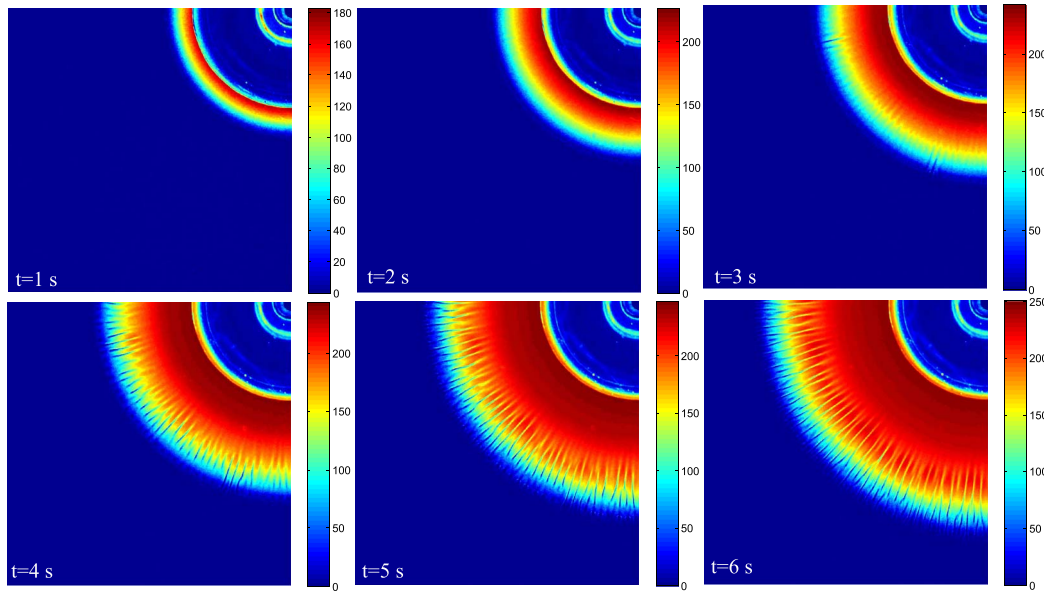


FIG. 3. Temporal evolution of the viscously stable miscible displacement of dyed water by glycerol 20 wt.% in a quarter of the Hele-Shaw cell at successive times shown in the lower left corner. The experimental pictures are represented using a gray scale map (false colors). The field of view is $2.5 \text{ cm} \times 2.5 \text{ cm}$.

B. Tip splitting and time evolution

To better illustrate the splitting of the stripes, we first plot the spatiotemporal map of the fluid displacement along a horizontal line passing through the injection point (Fig. 4(a)). From this plot, a given level of intensity I in grey values is selected and fitted with a power law $\xi(t) = \frac{qt^\epsilon}{\pi b}$, where ϵ is close to $1/2$. An example is shown in Fig. 4(b) for the $I = 100$ grey level. For a given time t_i , the intensity profile along the circular contour $\xi(t_i)$ is plotted. Two examples of selected contours are shown in Figs. 4(c) and 4(d) with the corresponding intensity profiles plotted in Figs. 4(e) and 4(f).

We see that the pattern, well defined at $t = 6 \text{ s}$, seems to later lose its regularity due to splitting events. The increasing effect of diffusion when Pe decreases leads to a lower intensity level and a blurry pattern further from the injection point as shown for $t = 16 \text{ s}$ for example.

C. Influence of the flow rate

The influence of the flow rate q is next investigated to see how the displacement velocity can influence the pattern (see Fig. 5). The first important observation is that the onset times are roughly the same (3–4 s) regardless of the speed of the flow, which is consistent with the fact that the Rayleigh number (5) proposed to quantify the instability is independent of the flow rate q . Nevertheless, a minimum flow rate is needed to observe the instability. Indeed, the Péclet number Pe cannot be too small otherwise vertical mixing by diffusion prevails and weakens the density gradient.

Comparing the different flow rates in Fig. 5, we can notice that, for the smaller $q = 1.68 \text{ mL/min}$, the pattern is quite blurry and the miscible interface more diffuse as the effect of diffusion is relatively more important. For the two larger flow rates, the filaments have sharper contours. Small dots, visible at the end of the white region where both fluids are mixing (rectangular frames of Fig. 5), might be interpreted as the final end of the 3D convection rolls. Splitting phenomena are visible at $t = 5 \text{ s}$ for the two larger displacement speeds and at $t = 6 \text{ s}$ for the smaller one where it is less easy to identify since the pattern is less contrasted.

To quantify the influence of the flow rate on the wavelength λ of the stripes, we consider in each experiment the situation for which the miscible interface has covered the same radial distance R after a given time t_{obs} . On the corresponding experimental picture, we evaluate on a half-circle of radius

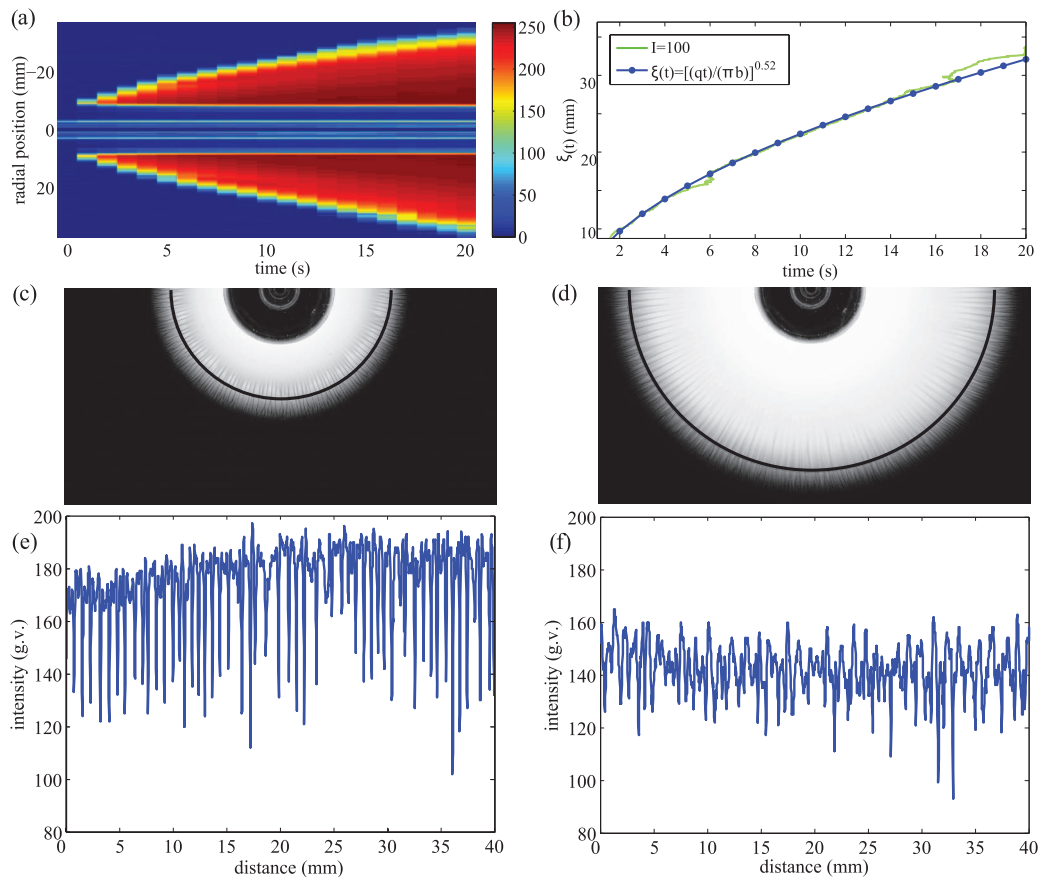


FIG. 4. (a) Spatiotemporal plot along a line passing through the injection point and (b) contour level $I = 100$ in grey values as a function of time in light gray (green) and fit $\xi(t)$ connected dots (blue), (c) and (d) experimental snapshots with the contour $\xi(t_i)$ plotted in black for $t_i = 6$ s and $t_i = 16$ s, respectively. (e) and (f) Intensity profiles along 40 mm of the black half-circle shown in (c) and (d).

R as shown in Fig. 6 the number N of intervals between two stripes. The different radii chosen are $R_1 = 1.50$ cm, $R_2 = 1.63$ cm, and $R_3 = 1.75$ cm. The related averaged wavelength $\lambda_i = \pi R_i/N$ and Péclet numbers Pe_i (calculated with the formula (4) using the infinite dilution value of diffusivity of glycerol in water $D = 1.06 \times 10^{-9} \text{ m}^2 \text{ s}^{-1}$) are given in Table II for three different flow rates.

We see that the larger the radius at which the number of fingers is counted, i.e., the smaller the Pe number for each imposed flow rate, the smaller the wavelength, which indicates that tip splitting phenomena occur further from the injection point. On the other hand, comparing the two smaller Pe for the two smaller flow rates, the wavelengths are relatively close.

We note here a dual influence of Pe on the wavelength as the results of Table II indicate that smaller wavelengths (i.e., a more unstable system) occur for smaller Pe while there is a critical Pe below which stripes do not appear as the system is then dominated by diffusion. Another dual role of Pe has already been evidenced in viscous instabilities.^{22,23} Here the explanation can be understood as follows: recalling that we compare in Fig. 6 situations where the miscible interface has reached approximately the same position, this implies that for the smaller flow rate, it takes more time for the injected fluid to reach the same radius. As the onset time of the instability is not significantly affected by the flow rate, it means that, in the case of the smaller flow rate, the pattern is existing for a longer time. At the back of the front, diffusion has had time to play a stabilizing role, leading to a larger wavelength whereas the wavelength is smaller at the edge of the front. On the contrary for the larger flow rate, diffusion does not have time to smooth smaller wavelengths out and nearly the same wavelength is observed at both the back and the front of the miscible interface.

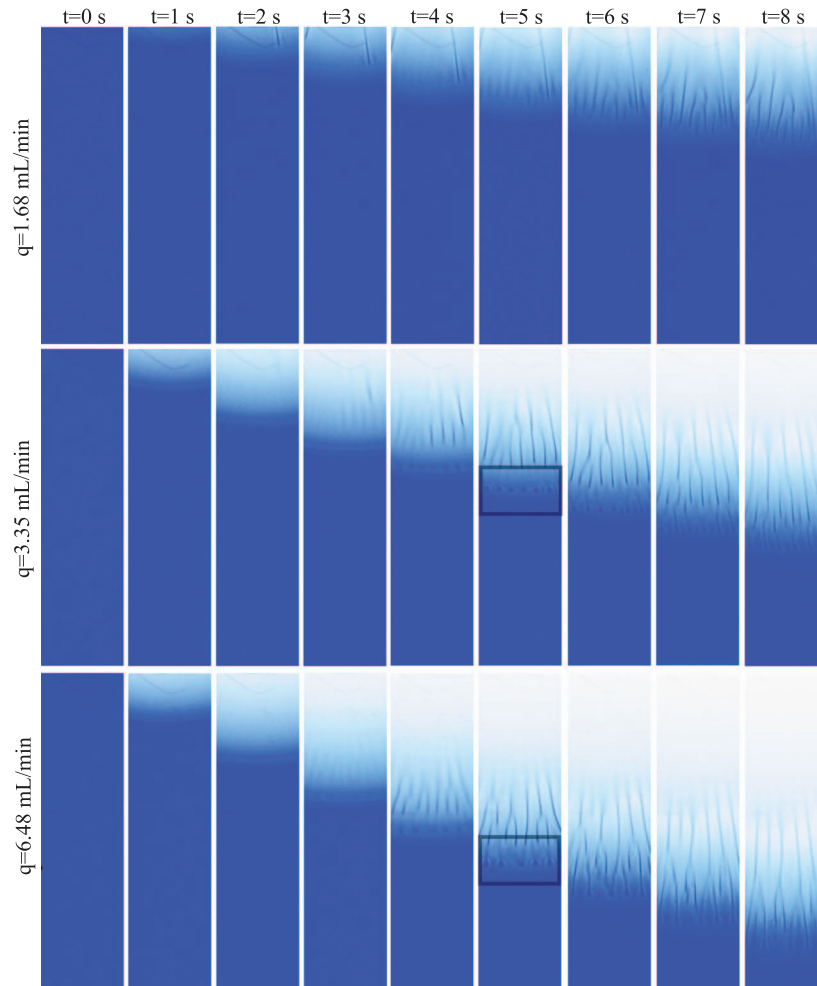


FIG. 5. Zoom on a selected region of the cell for t ranging from 0 to 8 s and for 3 different flow rates. The rectangles evidence the small dots visible in the mixing area, which might be the end of the convection rolls.

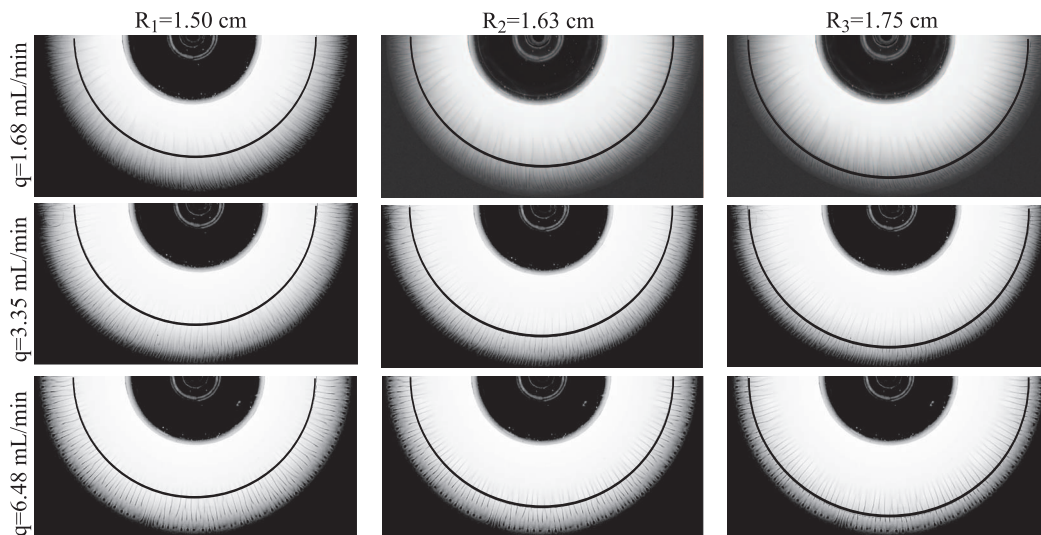


FIG. 6. Black half-circles of radius R_i on which the number N of wavelength λ is calculated. First line: $q = 1.68$ mL/min, $t = 15$ s; second line: $q = 3.35$ mL/min, $t = 9$ s; and third line: $q = 6.48$ mL/min, $t = 5$ s.

TABLE II. Averaged wavelength λ_i and related Péclet number Pe_i computed on the circles of radius R_i of Fig. 6 for three different flow rates. The different radii are $R_1 = 1.50$ cm, $R_2 = 1.63$ cm, and $R_3 = 1.75$ cm. The time t_{obs} is the time of the corresponding snapshot in Fig. 6.

q (mL/min)	t_{obs} (s)	Pe_1	$\lambda_1 \pm \Delta\lambda_1$ (mm)	Pe_2	$\lambda_2 \pm \Delta\lambda_2$ (mm)	Pe_3	$\lambda_3 \pm \Delta\lambda_3$ (mm)
1.68	15	280	0.98 ± 0.05	258	0.79 ± 0.03	240	0.57 ± 0.01
3.35	9	559	0.80 ± 0.03	514	0.79 ± 0.03	479	0.58 ± 0.01
6.48	5	1081	0.70 ± 0.02	995	0.71 ± 0.02	927	0.64 ± 0.02

As a summary, the experiments presented in this section show that when a denser and more viscous fluid is injected radially into a less dense and less viscous one in a horizontal Hele-Shaw cell, a pattern with stripes aligned in the direction of the flow is observed. The destabilization appears with an onset time that is independent of the flow rate. Furthermore, in the radial geometry, splitting phenomena occur beyond a certain time or equivalently beyond a given distance from the injection point, leading to a smaller wavelength.

V. INFLUENCE OF THE THICKNESS FOR CONSTANT RATIO q/b

Next, the influence of the thickness b of the gap of the Hele-Shaw cell on the wavelength of the pattern is studied for gaps ranging from 0.08 mm to 0.89 mm, for an aqueous solution of 20 wt.% glycerol injected into dyed water. For $b = 0.08$ mm, no pattern develops as shown in Fig. 7, indicating that a minimum thickness is necessary for the instability to develop. Patterns are observed starting from $b = 0.13$ mm.

The flow rate q is adjusted depending on the thickness in order to have the same ratio q/b for all experiments. Proceeding this way enables us to work with the same radial evolution of the velocity, u_r , given by Eq. (3), in all the experiments. The number of wavelengths, N , is counted along a circle close to the border of the stripes on a quarter of the cell. The related data are summarized in Table III for the experimental images shown in Fig. 8.

The measured wavelength, of the order of 0.7 mm, appears to be nearly independent of the gap width. This is due to the fact that the onset time is here short and therefore the distance \mathcal{L} on which the unfavorable density difference $\Delta\rho$ operates is still much smaller than the gap. We notice that for this set of data, the wavelength of the pattern is of the order of the gap of the cell or a bit larger. Comparison with theoretical predictions in the viscously unstable case⁶ is however difficult as the values of the parameters are different.

VI. INFLUENCE OF THE RELATIVE FLUID PROPERTIES

In the experiments presented in Secs. IV and V, glycerol 20 wt.% is injected in dyed water and differences in both density and viscosity between the two liquids are present. In order to isolate the role played by these two parameters independently, we have first performed a set of experiments

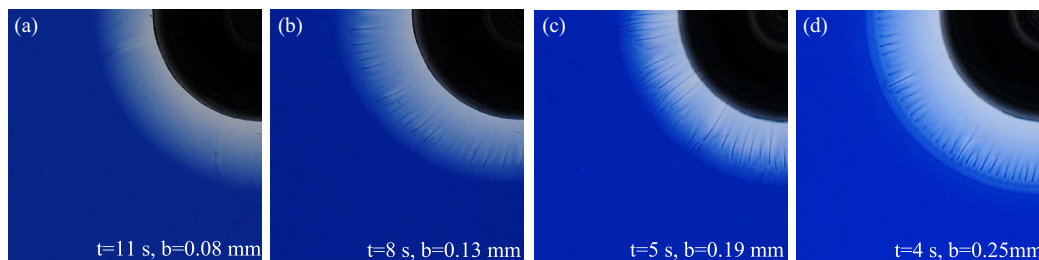


FIG. 7. Buoyancy pattern for the four smaller thicknesses available. The field of view is $2\text{ cm} \times 2\text{ cm}$ and the flow rates are, respectively, (a) $q = 0.52$ mL/min, (b) 0.85 mL/min, (c) 1.25 mL/min, and (d) 1.64 mL/min.

TABLE III. Influence of the gap thickness on the wavelength of the pattern. The ratio q/b is kept constant and λ is evaluated along a quarter of a circular contour with radius R .

Thickness (mm)	Onset time (s)	R (cm)	N (number of λ)	$\lambda \pm \Delta\lambda$ (mm)
0.25	3	1.4	32	0.69 ± 0.04
0.33	3	1.6	36	0.70 ± 0.04
0.38	2	1.4	30	0.73 ± 0.05
0.46	3	1.5	35	0.67 ± 0.04
0.51	2	1.6	33	0.76 ± 0.05
0.59	3	1.5	32	0.74 ± 0.05
0.64	3	1.6	39	0.64 ± 0.03
0.70	2	1.5	32	0.74 ± 0.05
0.76	3	1.6	45	0.56 ± 0.03
0.89	3	1.6	31	0.80 ± 0.05

where $\mu_2/\mu_1 \approx 1$ for different values of $\Delta\rho/\rho_1$ to study the role of density. Next, to isolate the influence of the viscosity, we have considered cases where $\Delta\rho/\rho_1$ is fixed and $\mu_1 \approx \mu_2$ is increased. Finally, we vary both viscosity and density by considering glycerol in different concentrations injected in dyed water.

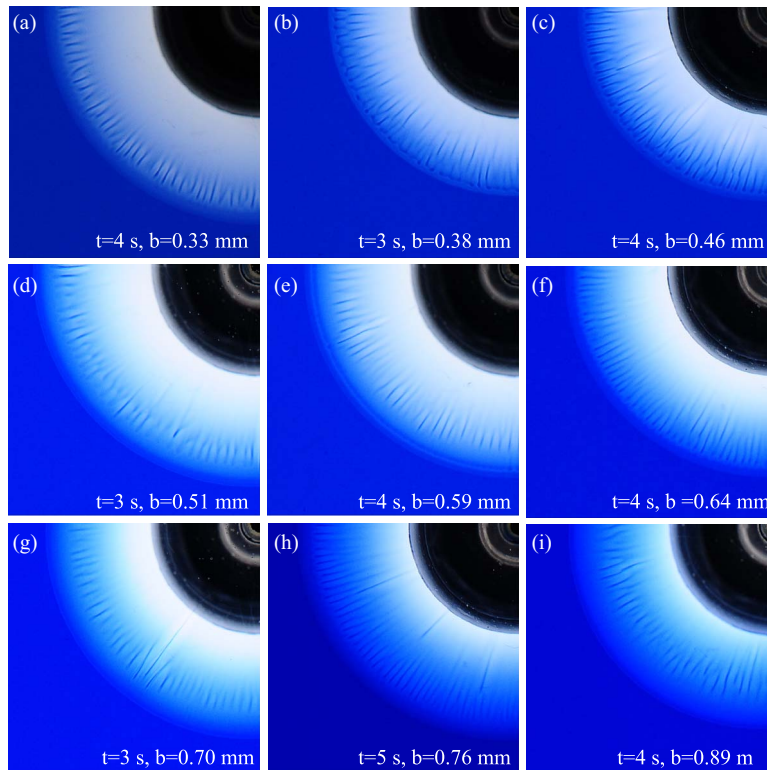


FIG. 8. Instability pattern for different thicknesses b and the same injection velocity at constant q/b . The experimental pictures correspond to the first picture where a clear pattern is observed (1 s after destabilization). The field of view is $2\text{ cm} \times 2\text{ cm}$. The flow rates are the following: (a) $q = 2.17\text{ mL/min}$, (b) 2.50 mL/min , (c) 2.82 mL/min , (d) 3.35 mL/min , (e) 3.88 mL/min , (f) 4.20 mL/min , (g) 4.60 mL/min , (h) 4.99 mL/min , and (i) 5.85 mL/min .

TABLE IV. Fluid properties for the smallest and the largest density ratios.

Solutions	$\Delta\rho/\rho_1$	μ_1 (cP)	μ_2/μ_1
Smallest density ratio	1×10^{-3}	1.02	0.98
Largest density ratio	20×10^{-3}	1.16	0.86

A. Viscosity ratio close to unity, variable $\Delta\rho/\rho_1$

A way to confirm that the instability under study is due to buoyancy is to take the relative density between the two fluids as a variable parameter, keeping the viscosity ratio close to unity. When the parameter $\Delta\rho/\rho_1$ is close to zero, the system should remain stable whereas increasing the density difference should lead to a more unstable situation and the onset time of the pattern should be smaller. To check this, we have set up a series of experiments in which a low concentration sucrose solution is injected in dyed water in a cell with 0.51 mm gap thickness. For the smallest value of $\Delta\rho/\rho_1$, the viscosity μ_1 is 1.02 cP, so that the viscosity ratio is $\mu_2/\mu_1 = 1/1.02 \approx 0.98$, whereas for the largest value of density contrast, the viscosity μ_1 is 1.16 cP and $\mu_2/\mu_1 = 1/1.16 \approx 0.86$. The relative error made in assuming that the viscosity ratio is 1 will be 2% for the smallest density contrast and 14% for the largest one (Table IV).

The onset times are plotted as a function of $\Delta\rho/\rho_1$ for two different flow rates in Fig. 9 on a log-log scale. We see that the smaller $\Delta\rho/\rho_1$, the larger the onset time which is consistent with the hypothesis of destabilization by buoyancy and with the expected increase of the growth rate with Rayleigh number. In particular, the power law of approximately -1.0 is consistent with a growth rate that is proportional to Ra .

Comparing the trends for the two flow rates shows however that the onset time does not change significantly with the speed of the flow, as it was shown previously in Sec. IV. This proves that it is the relative properties of the fluids which are mainly determining the instability. In addition, the pattern is qualitatively the same whether aqueous solutions of sucrose or not too concentrated glycerol solutions are used.

B. Viscosity ratio close to unity for increasing values of μ , constant $\Delta\rho/\rho_1$

We next examine the influence of an increased viscosity when keeping $\mu_1 \approx \mu_2$ and $\Delta\rho/\rho_1$ constant. In order to do so, we have performed a set of experiments with glycerol solutions of different concentrations. Once prepared, the solution is split into two parts. The first one is dyed with 0.06 wt.% Trypan blue. The second one is kept transparent and sucrose is added to it in order to obtain a value of $\Delta\rho/\rho_1$ close to 5×10^{-3} . This small addition of sucrose is assumed not to change

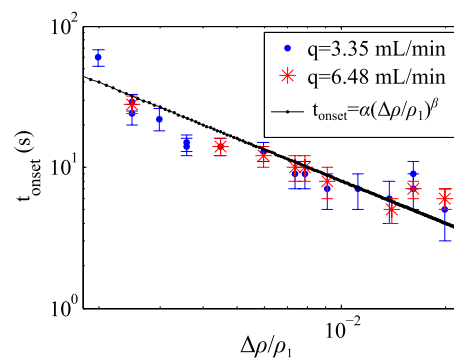


FIG. 9. Onset times for two different flow rates as a function of $\Delta\rho/\rho_1$ on a log-log scale. The fluid 1 is a sucrose solution and fluid 2 is dyed water. Dots (blue) correspond to $q = 3.35$ mL/min, stars (red) to $q = 6.48$ mL/min, and the black dotted line to a fit of the experimental data. The values of the power law fit are $\alpha = 0.08$ and $\beta = -1$.

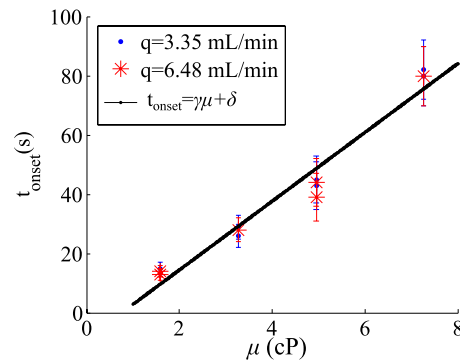


FIG. 10. Onset times for two different flow rates as a function of the dynamical viscosity $\mu \approx \mu_1 \approx \mu_2$. Fluids 1 and 2 are prepared from the same initial glycerol solution. A small amount of sucrose is added in fluid 1 such that $\Delta\rho/\rho_1 \approx 5 \times 10^{-3}$ while the dye is added in fluid 2. Dots (blue) correspond to $q = 3.35$ mL/min, stars (red) to $q = 6.48$ mL/min, and the black dotted line to a fit of the experimental data. The linear fit coefficients are $\gamma = 11.6$ and $\delta = -8.8$.

the viscosity of the glycerol solution. For an aqueous solution of sucrose injected in dyed water, ρ_1 has to be equal to 1.005 g cm^{-3} to obtain $\Delta\rho/\rho_1 = 5 \times 10^{-3}$ at $T=20^\circ\text{C}$, and the extrapolated viscosity²¹ is $1.028 \text{ cP} < \mu_1 < 1.055 \text{ cP}$. For these data, the maximum error made assuming $\mu_1 = 1 \text{ cP}$ is 5.5%.

Fig. 10 shows that the larger the viscosity, the larger the onset time of the buoyancy-driven stripes for a fixed value of $\Delta\rho/\rho_1$, which seems logical as the larger the viscosity, the more difficult it is to induce fluid motion. In a manner similar to the dependence on the density difference, the nearly linear dependence on viscosity is consistent with a scaling of the instability growth rate with the Rayleigh number, as smaller μ indicates larger growth rate (shorter onset time) and vice versa.

C. Influence of changing both $\Delta\rho/\rho_1$ and μ_2/μ_1

Eventually, we go back to the case where both effects of density and viscosity are present (see Table V) when glycerol solutions are injected in dyed water for two different concentrations (5 and 20 wt.%). The thickness of the gap is 0.51 mm and the flow rate $q = 6.48$ mL/min. Fig. 11 shows that the larger the concentration of glycerol, the earlier the destabilization occurs.

The number of stripes, N , is counted along a circle of radius $R = 2.1$ cm. The results for the average wavelength λ are summarized in Table V. From these data, we see that the larger the density of the injected solution, the smaller the wavelength. Since the destabilization is occurring earlier for larger density differences, splitting events have had time to occur and the resulting λ is smaller.

Other combinations of fluids have been studied to test cases where now it is the properties of the displaced fluid which are changed: 48 wt.% glycerol solutions plus sucrose injected either in dyed 48 wt.% glycerol solution or dyed 17 wt.% glycerol solution, for comparison. The corresponding images are shown in Fig. 12 and the properties of the two fluids are reported in Table VI. Fig. 12 clearly shows that for $\Delta\rho/\rho_1 = 5 \times 10^{-3}$ the miscible interface is not yet unstable at $t = 8$ s whereas for $\Delta\rho/\rho_1 = 71 \times 10^{-3}$, the pattern is already developing at $t = 4$ s. These results indicate that, when keeping the same injected solution, reducing the concentration of the displaced fluid leads to a more unstable situation. In conclusion, decreasing the ratio $\Delta\rho/\rho_1$ is a way of delaying the instability.

TABLE V. Influence of the fluid properties on the wavelength λ of the pattern computed along a circular contour with radius $R = 2.1$ cm at a time t_{obs} .

Solutions	ρ_1 (g cm ⁻³)	$\Delta\rho/\rho_1$	μ_1 (cP)	μ_2/μ_1	t_{obs} (s)	$\lambda \pm \Delta\lambda$
Glycerol 5 wt.% → dyed water	1.0115	11×10^{-3}	1.05	0.95	9	0.97 ± 0.06
Glycerol 20 wt.% → dyed water	1.0479	46×10^{-3}	1.80	0.56	9	0.80 ± 0.04

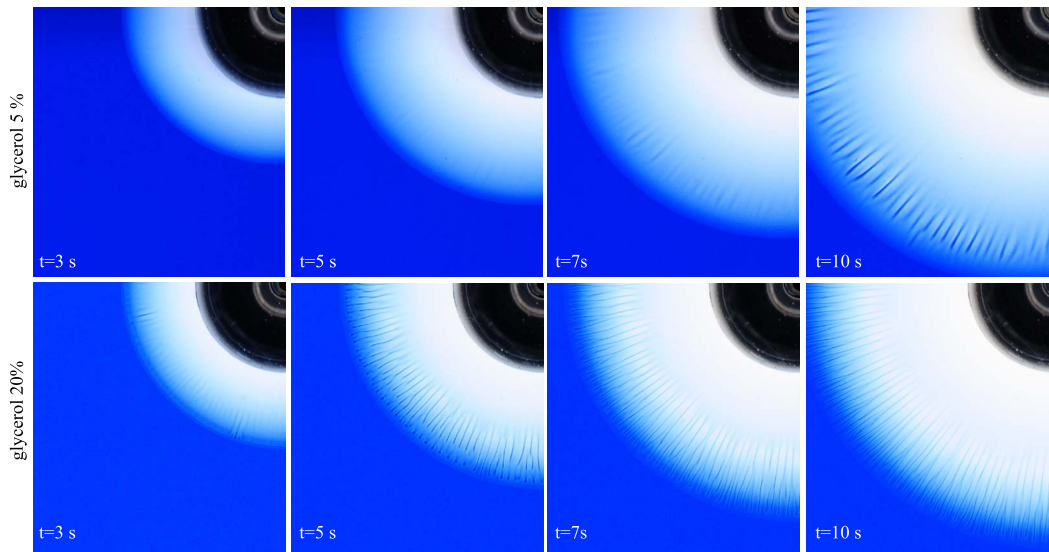


FIG. 11. Temporal evolution of the miscible displacement of dyed water by glycerol solutions for two different concentrations: first line $C_1 = 5$ wt.% and second line: $C_1 = 20$ wt.%. The field of view is $2.4 \text{ cm} \times 2 \text{ cm}$ and the flow rate $q = 6.48 \text{ mL/min}$.

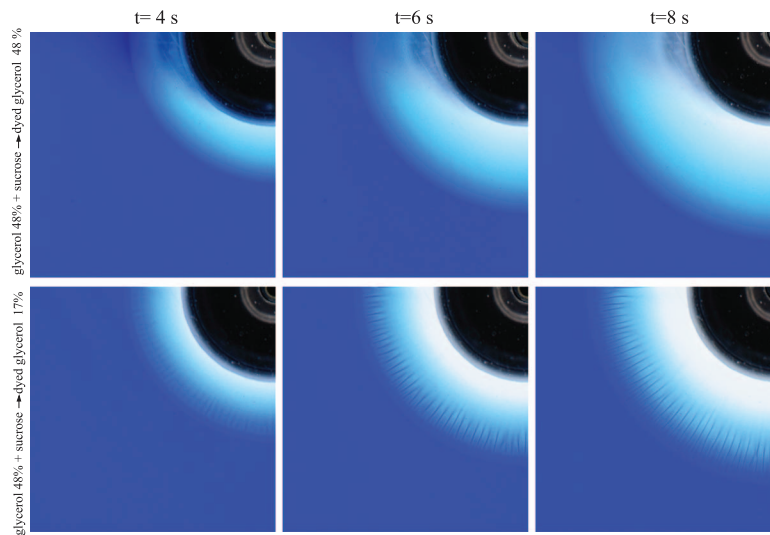


FIG. 12. Experimental pictures of miscible interfaces at different times. First line: glycerol 48 wt.% + sucrose injected in dyed glycerol 48 wt.%. Second line: glycerol 48 wt.% + sucrose displacing dyed glycerol 17 wt.%. The field of view is $2 \text{ cm} \times 2 \text{ cm}$ and the flow rate $q = 6.48 \text{ mL/min}$.

TABLE VI. Fluid properties with glycerol 48 wt.% as the injected fluid.

Solutions	ρ_1 (g cm $^{-3}$)	$\Delta\rho/\rho_1$	μ_1 (cP)	μ_2/μ_1	t_{onset}
Glycerol 48 wt.% + sucrose \rightarrow dyed glycerol 17 wt.%	1.1224	71×10^{-3}	4.95	0.31	3
Glycerol 48 wt.% + sucrose \rightarrow dyed glycerol 48 wt.%	1.1224	5×10^{-3}	4.95	≈ 1	Infinite

If the viscosity is roughly the same for the two fluids with a constant $\Delta\rho/\rho_1$, larger viscosities also delay the onset time of the pattern.

VII. CONCLUSIONS

We have presented an experimental study of a buoyancy-driven instability observed when injecting a viscous fluid into another miscible less viscous one within a horizontal Hele-Shaw cell. Even if the displacement is viscously stable, a pattern consisting of very thin stripes oriented perpendicularly to the miscible interface develops provided the density difference between the two solutions and the gap of the cell are large enough. The phenomenon is related to buoyancy as it disappears in a vertical cell. It can be explained in terms of a buoyancy-driven instability of the density profile which is stretched in the gap of the cell in the course of time by the fluid injection. In a horizontal cell with radial injection, the pattern, which appears after a given onset time, consists of radial stripes. Further away from the injection point, splitting of the stripes is observed.

A parametric study shows that the system is more unstable when the density difference between the two fluids is increased at a constant μ and that the later the instability develops, the larger the wavelength. In parallel, at constant $\Delta\rho/\rho_1$, increasing the viscosity $\mu_1 \approx \mu_2$ has a stabilizing effect. These two dependencies, together with their scaling laws, are fully consistent with an instability growth rate proportional to $\Delta\rho/(\rho_1\mu)$, i.e., to a Rayleigh number. When both density and viscosity differences exist, for example, comparing cases of increasing concentrations of a given solute, the destabilization occurs earlier for the most concentrated solution. Changing the flow rate q does not have a significant influence on the onset time of the pattern but a minimum q is needed for the instability to be observed. Changing the thickness b of the cell keeping q/b constant does not have a significant influence on the instability as the onset time and the wavelength of the pattern for similar displacements are approximately constant. However, the pattern does not appear if the gap width is too small.

All these experimental observations can be rationalized by quantifying the instability in terms of a Péclet number Pe and a Rayleigh number Ra defined in Eqs. (4) and (5), respectively. Both parameters have to be larger than a critical value for the instability to set in. All effects which increase the Rayleigh number (increasing $\Delta\rho/\rho_1$ or decreasing μ) have a destabilizing effect. The existence of a threshold value in Ra explains why a given delay after the start of the injection is needed for the instability to set in. The Rayleigh number is independent of the gap width b and flow rate q which explains why these two parameters have no influence on the characteristics of the pattern once the system is unstable. Nevertheless, the gap width and flow rate must be large enough for the instability to develop. This is tantamount to say that the Péclet number of the problem must be large enough for the locally buoyantly unstable density gradient to develop within the stretched profile in the gap. If the flow rate and hence the Péclet number is too small or if the gap width is not large enough, then diffusion takes over the advective deformation of the profile and no instability sets in.

As future work, it would be of interest to conduct more experiments in a rectilinear displacement to isolate the influence of the injection speed on the problem. Indeed, in radial geometries, the speed decreases when the distance r from the injection point increases which complicates the interpretation of the mechanism at the origin of tip splittings for instance. Also it would be interesting to test the influence of the thickness b of the gap for different fluid pairs or for constant q rather than constant q/b . Results of experiments in rectilinear displacements could also be easier to compare with theoretical stability analyses or full numerical solutions of the relevant equations.^{6,7} Simulations could moreover test the influence of the different parameters of the problem on the evolution of the pattern in 3D.

ACKNOWLEDGMENTS

We acknowledge E. Meiburg and R. Oliveira for fruitful discussions and EU-ITN “Multiflow” Marie Curie network for financial support. A.D. and B.K. benefit from the financial support of the ARC CONVINCEN programme of the Communauté française de Belgique. A.D. and F.H. acknowledge financial support of Prodex.

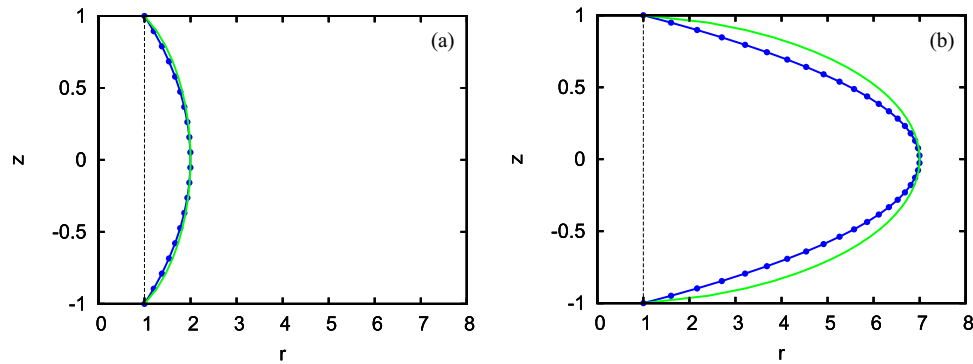


FIG. 13. Comparison of the interface profiles for rectilinear injection (dotted line/blue) and radial injection (full line/green) at two different dimensionless distances reached by the middle of the front (respectively represented in (a) and (b)). The coordinates are normalized by half the gap width and the injection location is $r = 1$.

APPENDIX: VELOCITY AND CONCENTRATION PROFILES WITHIN THE GAP OF A HELE-SHAW CELL FOR A RADIAL INJECTION

As shown in Refs. 19 and 20, the velocity field adopted by a flow injected radially between parallel plates is given (in the creeping regime) by

$$u_r(r, z) = \frac{3q}{8\pi b^3 r} (a^2 - z^2), \quad (\text{A1})$$

where $a = \frac{b}{2}$. According to this relation, the radial coordinate r of fluid particles then obeys the following equation:

$$\frac{dr}{dt} = \frac{3q}{8\pi b^3 r} (a^2 - z^2). \quad (\text{A2})$$

Starting from a cylindrical interface located at $r = r_{\text{inj}}$ at $t = 0$, we see that at time t , this interface is described by the following expression:

$$r^2 + Ctz^2 = Ca^2t + r_{\text{inj}}^2, \quad (\text{A3})$$

where $C = \frac{3q}{4\pi a^3}$. Equation (A3) describes an ellipse in the (r, z) coordinate system.

In Fig. 13, we compare the shapes of a parabolic velocity profile arising in the case of rectilinear injection and the elliptic profile arising in the case of radial injection. To allow an easy comparison, the profiles are compared when the tip of the injected fluid zone has reached the same distance from the injection point on the middle plane of the cell.

- ¹G. M. Homsy, "Viscous fingering in porous media," *Annu. Rev. Fluid Mech.* **19**, 271 (1987).
- ²J. Fernandez, P. Kurowski, P. Petitjeans, and E. Meiburg, "Density-driven unstable flows of miscible fluids in a Hele-Shaw cell," *J. Fluid Mech.* **451**, 239 (2002).
- ³F. Graf, E. Meiburg, and C. Härtel, "Density-driven instabilities of miscible fluids in a Hele-Shaw cell: linear stability analysis of the three-dimensional Stokes equations," *J. Fluid Mech.* **451**, 261 (2002).
- ⁴J. Martin, N. Rakotomalala, and D. Salin, "Gravitational instability of miscible fluids in a Hele-Shaw cell," *Phys. Fluids* **14**, 902 (2002).
- ⁵N. Goyal and E. Meiburg, "Unstable density stratification of miscible fluids in a vertical Hele-Shaw cell: influence of variable viscosity on the linear stability," *J. Fluid Mech.* **516**, 211 (2004).
- ⁶L. Talon, N. Goyal, and E. Meiburg, "Variable density and viscosity, miscible displacements in horizontal Hele-Shaw cells. Part 1. Linear stability analysis," *J. Fluid Mech.* **721**, 268 (2013).
- ⁷M. O. John, R. M. Oliveira, F. H. C. Heussler, and E. Meiburg, "Variable density and viscosity, miscible displacements in horizontal Hele-Shaw cells. Part 2. Nonlinear simulations," *J. Fluid Mech.* **721**, 295 (2013).
- ⁸S. Obernauer, "Inestabilidades entre fluidos miscibles en medios porosos," Ph.D. thesis (Universidad de Buenos Aires, 1999).
- ⁹R. Maes, "Experimental study of viscous fingering of miscible fluids in a Hele-Shaw cell," Ph.D. thesis (Université Libre de Bruxelles, 2010).
- ¹⁰D. Snyder and S. Tait, "A flow front instability in viscous gravity currents," *J. Fluid Mech.* **369**, 1 (1998).

- ¹¹ P. Garik, J. Hetrick, B. Orr, D. Barkey, and E. Ben Jacob, "Interfacial cellular mixing and a conjecture on global deposit morphology," *Phys. Rev. Lett.* **66**, 1606 (1991).
- ¹² S. H. Hejazi, P. M. J. Trevelyan, J. Azaiez, and A. De Wit, "Viscous fingering of a miscible reactive $A + B \rightarrow C$ interface: a linear stability analysis," *J. Fluid Mech.* **652**, 501 (2010).
- ¹³ Y. Nagatsu and A. De Wit, "Viscous fingering of a miscible reactive $A + B \rightarrow C$ interface for an infinitely fast chemical reaction: Nonlinear simulations," *Phys. Fluids* **23**, 043103 (2011).
- ¹⁴ L. A. Riolfo, Y. Nagatsu, S. Iwata, R. Maes, P. M. J. Trevelyan, and A. De Wit, "Experimental evidence of reaction-driven miscible viscous fingering," *Phys. Rev. E* **85**, 015304(R) (2012).
- ¹⁵ A. Baker, Á. Tóth, D. Horváth, J. Walkush, A. S. Ali, and W. Morgan, "Precipitation pattern formation in the copper(II) oxalate system with gravity flow and axial symmetry," *J. Phys. Chem. A* **113**, 8243 (2009).
- ¹⁶ R. Maes, G. Rousseaux, B. Scheid, M. Mishra, P. Colinet, and A. De Wit, "Experimental study of dispersion and miscible viscous fingering of initially circular samples in Hele-Shaw cells," *Phys. Fluids* **22**, 123104 (2010).
- ¹⁷ J. W. Deardorff, "Gravitational instability between horizontal plates with shear," *Phys. Fluids* **8**, 1027 (1965).
- ¹⁸ K. S. Gage and W. H. Reid, "The stability of thermally stratified plane Poiseuille flow," *J. Fluid Mech.* **33**, 21 (1968).
- ¹⁹ S. D. R. Wilson, "A note on laminar radial flow between parallel plates," *Appl. Sci. Res.* **25**(1), 349 (1972).
- ²⁰ J. D. Jackson and G. R. Symmons, "An investigation of laminar radial flow between two parallel discs," *Appl. Sci. Res.* **15**, 59 (1965).
- ²¹ W. M. Haynes, *CRC Handbook of Chemistry and Physics*, 92nd ed. (CRC Press, Boca Raton, FL, 2011).
- ²² R. M. Oliveira and E. Meiburg, "Miscible displacements in Hele-Shaw cells: three-dimensional Navier-Stokes simulations," *J. Fluid Mech.* **687**, 431 (2011).
- ²³ R. M. Oliveira and E. Meiburg, "Three-dimensional vorticity configurations in miscible Hele-Shaw displacements," *Proc. IUTAM* **7**, 203 (2013).